Applied Radiation and Isotopes 229 (2026) 112381

Contents lists available at ScienceDirect

Applied Radiation and Isotopes

journal homepage: www.elsevier.com/locate/apradiso

Analysis of dosimetric characteristics of $CaSO_4$:Mn,Tb phosphors synthesized by four different routes

Anderson M.B. Silva [a,*], Danilo O. Junot [b], Patrícia L. Antonio [a], Divanizia N. Souza [c], Linda V.E. Caldas [a]

[a] Instituto de Pesquisas Energéticas e Nucleares, Comissão Nacional de Energia Nuclear, IPEN/CNEN-SP, Av. Prof. Lineu Preste, São Paulo, SP, Brazil
[b] Instituto de Física Armando Dias Tavares, Universidade do Estado do Rio de Janeiro, Rio de Janeiro, RJ, Brazil
[c] Departamento de Física, Universidade Federal de Sergipe, Marechal Rondon, São Cristovão, SE, Brazil

ARTICLE INFO

Keywords:
Radiation detection and measurement
Thermoluminescence
Optically stimulated luminescence
$CaSO_4$:Mn,Tb
Synthesis methods

ABSTRACT

The luminescence properties of crystalline materials are critical for monitoring physical phenomena, including ionizing radiation doses. In this study, $CaSO_4$:Mn,Tb phosphors were synthesized using four distinct methods: solid-state diffusion, co-precipitation, sol-gel, and slow evaporation routes. The influence of synthesis conditions on the structural, morphological, elemental, and luminescent properties of the phosphors was systematically investigated. X-ray diffraction (XRD) patterns confirmed that all synthesis routes produced samples with a stable $CaSO_4$ crystal phase, and doping with Tb^{3+} and Mn^{2+} did not alter the crystal structure. Scanning electron microscopy (SEM) images revealed that synthesis methods significantly influenced grain morphology. Energy-dispersive X-ray spectroscopy (EDS) spectra validated the successful incorporation of Tb^{3+} and Mn^{2+} ions into the crystal lattice. The slow evaporation route, followed by co-precipitation, yielded the highest intensity of thermoluminescence (TL) glow curves, which were characterized using Schott BG-39 and Hoya U-340 bandpass filters to control wavelengths. Different emission curve behaviors for TL were observed. In the optically stimulated luminescence (OSL) analyses, obtained with continuous intensity optical stimulation and a 40 s integration time, all samples exhibited an exponential decrease in OSL signal as the charge traps were emptied. The $CaSO_4$:Mn,Tb phosphor produced via the sol-gel route, and that synthesized by slow evaporation, showed the highest OSL intensity, followed by those produced via co-precipitation and solid-state synthesis. However, the high coefficient of variation (CV) in TL/OSL responses of samples produced by sol-gel and co-precipitation methods limited the reproducibility of the luminescent measurements. The slow evaporation route emerged as the most consistent and efficient method, exhibiting low CV values (<10 %) in terms of signal variation and sensitivity, the highest linear correlation in the dose-response relationship over the irradiation range of 0.16 Gy–100 Gy, and greater TL signal stability for long-term applications.

1. Introduction

In radiation dosimetry, significant research has focused on developing dosimeters that combine high sensitivity, excellent stability, and the ability to measure the dose received with sufficient reproducibility and reasonable accuracy across the full range of energies, doses, and dose rates expected during its use (Poston, 2003). These dosimeters are designed to be suitable for environments where radiation levels can vary significantly. Among the most widely used techniques for radiation monitoring are thermoluminescence (TL), optically stimulated luminescence (OSL), and electron paramagnetic resonance (EPR), all of which provide accurate, reliable solutions for measuring radiation exposure.

Luminescent materials play a crucial role in radiation monitoring by absorbing energy from incident radiation over time and emitting light when triggered by external stimuli. Methods like TL and OSL utilize the phosphorescent properties of irradiated materials. In TL, heat prompts light emission, whereas OSL uses specific wavelengths of light for stimulation. The amount of light emitted correlates directly with the radiation absorbed, providing a reliable approach to accurately measure

This article is part of a special issue entitled: Reprolam 2024 published in Applied Radiation and Isotopes.

* Corresponding author.
E-mail address: andersonmanoel22@hotmail.com (A.M.B. Silva).

https://doi.org/10.1016/j.apradiso.2025.112381
Received 20 December 2024; Received in revised form 16 October 2025; Accepted 16 December 2025
Available online 16 December 2025

radiation doses (Sen et al., 2024).

Over the past two decades, sulfate-based phosphor materials doped with lanthanide and metal elements have garnered attention due to their potential in advanced technologies, such as light-emitting diodes, sensors, and radiation monitoring (Aboelezz et al., 2022; Bastani et al., 2019; Dhoble et al., 2003; Gaikwad et al., 2016; Lakshmanan et al., 2006; More et al., 2015; Najar et al., 2023; Tang et al., 2006). Among the most studied sulfates are lithium sulfate (Li_2SO_4), strontium sulfate ($SrSO_4$), magnesium sulfate ($MgSO_4$), sodium sulfate (Na_2SO_4), barium strontium sulfate ($BaSrSO_4$), potassium sulfate (K_2SO_4) and calcium sulfate ($CaSO_4$), all of which show promising luminescent properties for these applications.

The synthesis methods for $CaSO_4$, including co-precipitation, sol-gel, recrystallization, wet chemistry, solid-state diffusion, and slow evaporation, are crucial for enhancing its dosimetric properties. These methods have been extensively studied and documented (Bahl et al., 2017; Guckan et al., 2017; Junot et al., 2011, 2014, 2016, 2019, 2020, 2024; Kadari et al., 2016; Silva et al., 2020, 2021, 2022, 2023, 2024, 2025).

Recent advances in doping $CaSO_4$ with rare earth elements, such as terbium (Tb) as a co-dopant in $CaSO_4$:Mn, have further improved its luminescent properties. For example, the co-doping of $CaSO_4$:Mn with Tb resulted in a TL glow curve with peaks at 205 °C and 325 °C, and a fading of only 17 % after 30 days. The co-doped samples showed reduced fading compared to the mono-doped ones, suggesting that the co-doping stabilizes charge recombination centers at deeper energy levels. Despite these improvements, a deeper understanding of the luminescent mechanisms and defect interactions is still required to fully optimize the use of $CaSO_4$:Mn,Tb in radiation dosimetry.

The study investigates the influence of four distinct synthesis methods (solid-state diffusion, co-precipitation, sol-gel and slow evaporation) on the structural, morphological and luminescent (TL and OSL) properties of $CaSO_4$:Mn,Tb phosphors. TL glow curves were recorded in both the ultraviolet (UV) and visible (VIS) spectral regions to evaluate spectral response of the phosphors. The TL and OSL results are compared with previously reported data for samples produced via the slow evaporation method (Silva et al., 2022). To our knowledge, this is the first comprehensive study to systematically evaluate the impact of these synthesis routes on the luminescent performance of $CaSO_4$:Mn,Tb under beta radiation. This study highlighting the pivotal role of microstructural variations in maximizing the potential of this phosphor for dosimetric applications.

2. Materials and methods

2.1. Solid state diffusion reaction

The preparation of $CaSO_4$:Mn,Tb was carried out via a solid-state diffusion reaction, following a procedure previously described by Rani et al. (2015). For the phosphor synthesis, the following raw materials were used: $CaSO_4{\cdot}2H_2O$, Tb_4O_7, and $Mn(NO_3)_2{\cdot}4H_2O$. The latter two compounds were dissolved in distilled water under magnetic stirring in a glass beaker. The desired amounts of Tb and Mn dopants were each added at a concentration of 0.1 mol%. The mixture was thoroughly homogenized. Subsequently, $CaSO_4{\cdot}2H_2O$ added to the solution. After complete stirring, the solution was dried in glass beakers placed in an oven at 180 °C for 2 h. The dried powder was then finely ground in an agate mortar, transferred to alumina crucibles, and sintered at 600 °C for 1 h.

2.2. Co-precipitation method

$CaSO_4$:Mn,Tb was prepared using the chemical co-precipitation method, following a procedure previously described by Salah et al. (2006). Appropriate quantities of calcium acetate ($Ca(CH_3CO_2)_2{\cdot}2H_2O$), Tb_4O_7, and $Mn(NO_3)_2{\cdot}4H_2O$ were dissolved in triply distilled deionized water. The solution was then mixed stoichiometrically with an ammonium sulfate ($(NH_4)_2SO_4$) solution in the presence of ethanol. The resulting precipitate was filtered out and washed several times with distilled water. The obtained powder was first placed in an oven at 100 °C for 2 h and subsequently annealed at 650 °C for 2 h.

2.3. Sol-gel method

The procedure follows the method outlined by Kadari et al. (2016), who used calcium chloride dihydrate ($CaCl_2{\cdot}2H_2O$) and ammonium sulfate ($(NH_4)_2SO_4$) as precursors. The calcium chloride solution was prepared by dissolving $CaCl_2{\cdot}2H_2O$ in distilled water and ethanol, stirring magnetically at room temperature. The ammonium sulfate solution was then slowly added to the $CaCl_2{\cdot}2H_2O$ solution, followed by the addition of the dopants Tb_4O_7 and $Mn(NO_3)_2{\cdot}4H_2O$ to the solution to form $CaSO_4$:Mn,Tb. The mixture was stirred to obtain a homogeneous precipitate. In this process, ethanol (C_2H_6O) is used as the solvent, H_2O as the hydrolysis reagent, and ammonia (NH_4OH) as the catalyst. The resulting white precipitate was washed with distilled water and ethanol, and then dried at 100 °C for 24 h to remove residual water and solvent content.

2.4. Slow evaporation method

$CaSO_4$:Mn,Tb samples were prepared using the slow evaporation method, a well-established technique for synthesizing sulfate crystals. The crystal growth parameters were determined based on previous studies (Junot et al., 2016, 2019; Silva et al., 2020). In this method, a solution containing calcium carbonate ($CaCO_3$), sulfuric acid (H_2SO_4), terbium oxide (Tb_4O_7), and manganese nitrate ($Mn(NO_3)_2{\cdot}4H_2O$) was prepared. The solution was heated to 375 °C using a heating mantle and maintained at this temperature until the acid had completely evaporated. Subsequently, the crystals were washed, ground, and sieved. The resulting powders were then calcined at 600 °C for 1 h.

2.5. Methods of characterization

The crystal structure of the sample was analyzed using a Rigaku X-ray diffractometer (RINT, 2000/PC) with Cu-Kα radiation, operating at 60 kV and 30 mA. The scanning range was 20°–80° (2θ), with step increments of 0.04°. Additionally, the size, morphology, and structure of the powder samples were examined with a JSM-IT700HR scanning electron microscope (SEM), equipped with an energy-dispersive spectroscopy (EDS) system, which was used to assess the elemental composition of the produced samples. The powders were uniformly mixed with polytetrafluoroethylene (Teflon) to enhance the material's mechanical strength and facilitate its handling during the luminescence characterizations by TL/OSL. After applying a uniaxial pressure of 0.5 tons, well-formed pellets were produced. These pellets were subsequently sintered at 400 °C for 1 h to improve their strength and stability. The final cylindrical pellets had a mass of 30 mg and a diameter of 4 mm.

The samples were irradiated with a $^{90}Sr/^{90}Y$ beta source, delivering a dose rate of 4.33 Gy/min and a maximum energy of 2.27 MeV, with a cumulative dose of 1 Gy. TL and OSL measurements were performed using a DA-20 model Risø TL/OSL reader system. For TL measurements, a heating rate of 5 °C/s was applied, with the temperature reaching up to 450 °C. For OSL measurements, the excitation light source consisted of blue light-emitting diodes with a wavelength of 470 nm, and signal acquisition lasted for 40 s. The detection system utilized Schott BG-39 bandpass filters (transmittance in the visible region between 320 and 480 nm) and Hoya U-340 filters (transmittance in the UV region between 260 and 400 nm) to select the emission wavelengths. The coefficient of variation (CV), also known as the relative standard deviation, was calculated as the ratio of the standard deviation (σ) to the mean (μ), multiplied by 100 to express the result as a percentage ($CV = (\sigma/\mu) \times 100$). In this study, the CV was calculated for the TL and OSL responses

obtained from five analyzed pellets.

3. Results and discussions

3.1. XRD analysis

Fig. 1 shows the XRD patterns of $CaSO_4$:Mn,Tb synthesized using solid-state diffusion reaction, co-precipitation, sol-gel methods, and the slow evaporation route. Compared with the ICDD standard card 00-037-1496, it was confirmed that the crystal phase of all samples corresponds to $CaSO_4$ indicating successful synthesis via all four methods. The incorporation of rare earth and metal dopants had minimal impact on the crystal structure of $CaSO_4$ suggesting that the dopants were incorporated into the lattice. The XRD patterns of the samples are characteristic of orthorhombic anhydrite structures, displaying peaks at 2θ angles consistent with those reported by Silva et al. (2022, 2023, 2024).

3.2. SEM analysis

The morphological analysis of the phosphor samples prepared by the different synthesis routes is shown in Fig. 2(a–d) at a 3300 times magnification. The grains synthesized using the solid-state diffusion route exhibit an irregular morphology, with fragmented appearances and poorly defined edges, indicating a rough surface texture and some degree of agglomeration. In contrast, the sol-gel route resulted in $CaSO_4$:Mn,Tb grains with an elongated and crystalline structure, characterized by a more defined morphology indicative of a structured growth process. Grains obtained via the slow evaporation method display a denser appearance with irregular surfaces and agglomerated shapes, reflecting variations in morphology throughout the sample. The co-precipitation route resulted in grains with a prismatic and elongated morphology, featuring well-defined edges and smooth surfaces, consistent with crystalline materials formed under controlled synthesis conditions. These variations in grain morphology are influenced by differences in reagents, thermal treatments, and synthesis methods, which can affect the final properties of the phosphor, including its luminescent performance and dosimetric response.

Fig. 3 presents the EDS spectra of $CaSO_4$:Mn,Tb synthesized by the four methods. The elemental composition analysis revealed prominent peaks for oxygen (O), sulfur (S), and calcium (Ca), confirming the presence of the primary reactants in the final material. Despite the low dopant concentrations (≤0.1 mol%), distinct signals for Tb and Mn were also detected. Additionally, the EDS mapping showed a uniform distribution of Tb and Mn elements over the surface, demonstrating the successful incorporation of the dopants into the crystal structure and highlighting the efficiency of the synthesis methods.

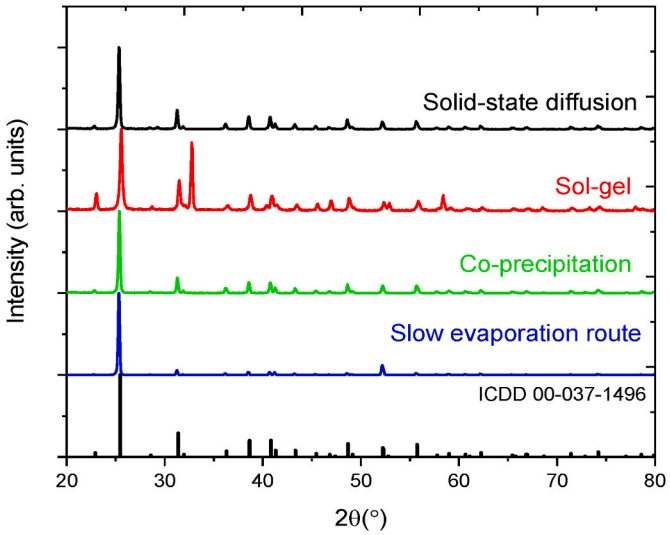

Fig. 1. XRD patterns of $CaSO_4$:Mn,Tb powders produced by different routes.

3.3. Thermoluminescence and optically stimulated luminescence studies

The adapted slow evaporation route successfully synthesized $CaSO_4$:Mn,Tb phosphors, with efficient incorporation of Mn^{2+} and Tb^{3+} ions into the crystal lattice. Structural defects introduced by doping enhanced the luminescent properties of the phosphor, as confirmed by the TL glow curve, which shows peaks at 205 °C and 325 °C, with only 9.6 % fading after 30 days, indicating stability (Silva et al., 2024). Comparative TL/OSL analysis with commercial dosimeters, such as TLD-100 and Al_2O_3:C, demonstrated competitive performance of the $CaSO_4$:Mn,Tb, with reliable and reproducible signals. The phosphors exhibited a linear luminescent response from a few mGy to 100 Gy, confirming their potential as cost-effective candidates for radiation dosimetry.

To investigate the impact of different synthesis routes on their luminescence properties, samples were irradiated with a 1 Gy beta radiation dose and subjected to a heating rate of 5 °C/s. TL and OSL signals were analyzed to identify the method that yields the highest luminescence sensitivity. TL emission curves were recorded and examined in both the ultraviolet (UV) and visible (VIS) regions, using Hoya U-340 (Fig. 4) and Schott BG-39 (Fig. 5) filters to isolate specific spectral components for detailed analysis. The analysis of the TL signals in the UV region revealed significant differences between the samples synthesized by different methods. The samples prepared by the slow evaporation route exhibited the highest TL emission intensity, standing out compared to the other methods. Three main peaks were identified, with the most intense peak located around 270 °C, suggesting the presence of deep electron traps associated with greater thermal stability of the emissions.

The sol-gel route resulted in the second-highest TL emission intensity, with a single well-defined and symmetrical peak at lower temperatures, located in the same region as the first peak observed for the slow evaporation route. The samples synthesized by co-precipitation, although displaying less intense peaks, showed good definition and positions close to those of the slow evaporation peaks, indicating a similarity in the structure of the electron traps formed. In contrast, the samples prepared by solid-state diffusion presented TL signals with poorly defined peaks and lower intensity, suggesting reduced efficiency in forming suitable electron traps.

The variations observed in the intensity and shape of the peaks are strongly influenced by crystal structure, synthesis method, grain size, and morphology (Nair et al., 2020). Among the methods evaluated, the slow evaporation route emerged as the most efficient, producing a homogeneous and well-integrated matrix with more effective charge traps for TL emission.

The TL emission curves in the VIS region also revealed clear differences in the luminescent behavior of samples synthesized by different methods. Similar to the samples analyzed using a UV filter, the one prepared by the slow evaporation route exhibited the highest TL intensity, maintaining distinct peaks that align with the results observed in the visible spectrum. The intensity of the emission remains significantly higher than that of samples prepared by other synthesis routes, further suggesting that slow evaporation results in samples with a set of electron traps more appropriate for a thermoluminescent material, with greater thermal stability, as evidenced by the peaks observed at higher temperatures. This stability minimizes undesired charge carrier release at elevated temperatures, enhancing the accuracy and reliability of radiation dose measurements. The co-precipitation method exhibited a lower TL intensity compared to the slow evaporation route, but it performed better than the solid-state diffusion and sol-gel methods. The co-precipitation samples still showed clear and well-defined TL signals, consistent with the peaks observed in the UV region. The samples synthesized by sol-gel and solid-state diffusion, although displaying lower

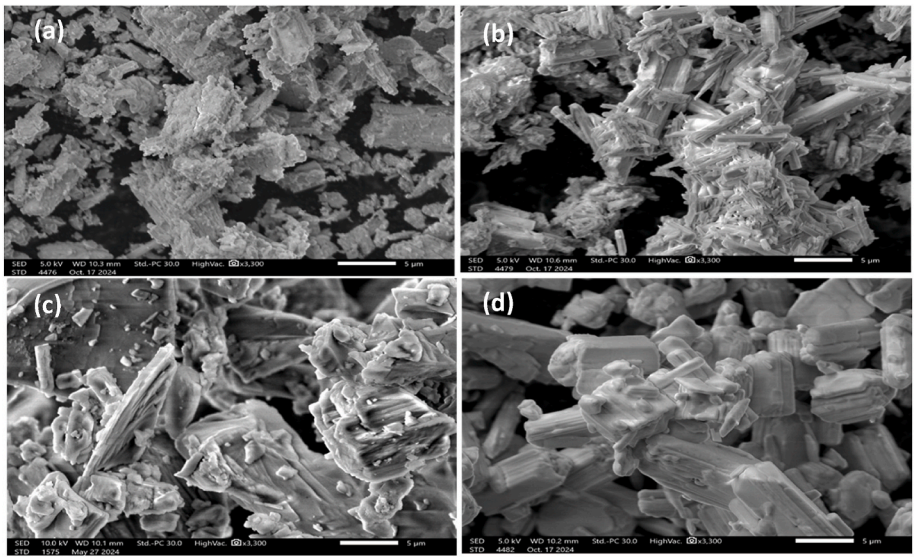

Fig. 2. SEM micrographs of $CaSO_4$ powders prepared using different synthesis routes: (a) Solid-state diffusion, (b) Sol-gel method, (c) Slow evaporation, and (d) Co-precipitation method.

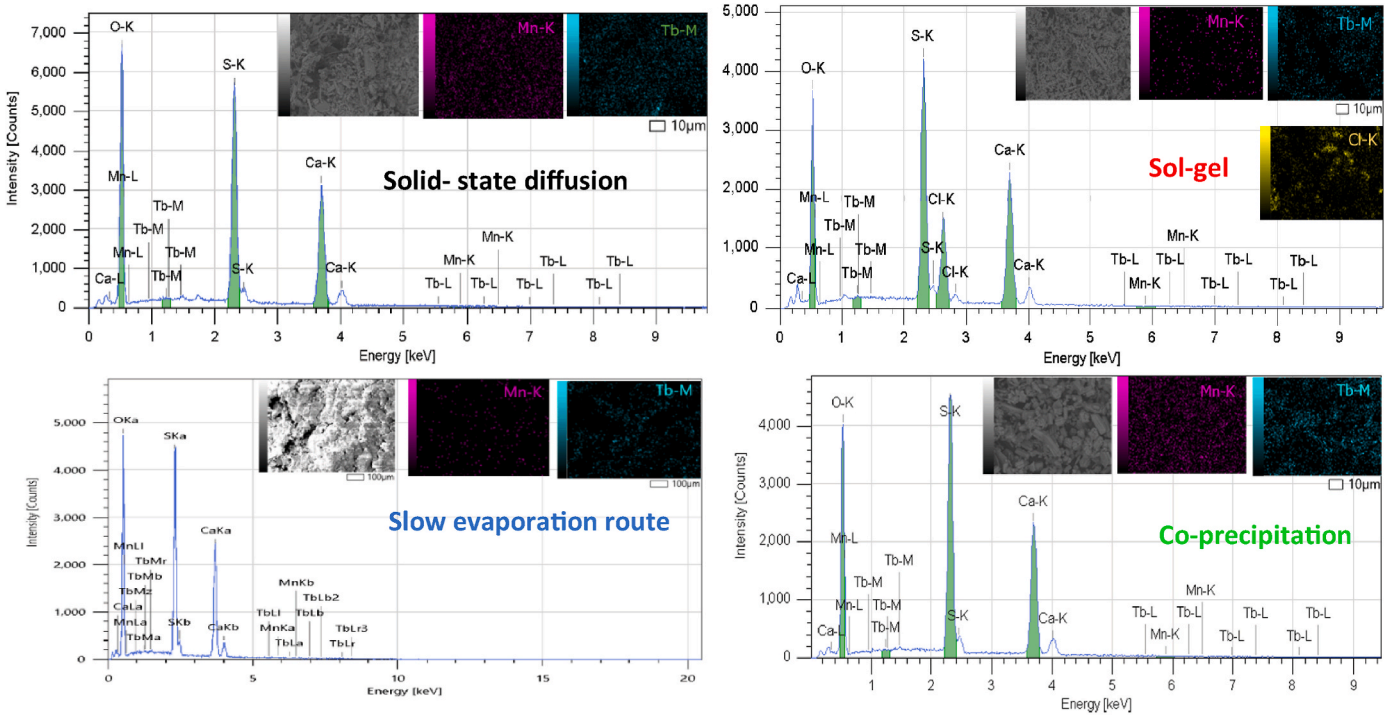

Fig. 3. EDS spectra of $CaSO_4$ samples and EDS mapping results of $CaSO_4$:$Mn_{0.1\ \%}$,$Tb_{0.1\ \%}$ synthesized via different routes.

intensity peaks in the UV region, still exhibited clear and well-defined signals. The peaks are distributed in the same temperature range as the TL emissions observed for the slow evaporation method. The results indicate that these methods, although less efficient in promoting TL intensity, are still capable of producing samples with electron traps that favor luminescent emission properties.

Fig. 6 illustrates the variation in the TL response, represented by the area under the TL emission curves, for samples synthesized using different methods. The observed trends emphasize the significant influence of the synthesis route on the luminescence efficiency of the samples. Among the methods evaluated, the slow evaporation route stands out, yielding the highest TL response across both spectral regions. This superior performance confirms the efficiency of this method in creating a matrix with highly effective electron traps. The co-precipitation method ranks second in TL response, demonstrating better performance compared to the sol-gel and solid-state diffusion methods. While the TL response of the samples is lower than that one produced by the slow evaporation method, the significant improvement over the other two methods indicates the co-precipitation route's ability to create moderately effective electron traps. Furthermore, the close agreement between the TL intensities obtained using Hoya U-340 and Schott BG-39 filters underscores the consistency of the results across the ultraviolet and visible regions. This consistency indicates that the trends in TL response are not limited to a specific wavelength range, but reflect the general luminescence efficiency of the synthesized samples.

Fig. 7 presents the continuous wave OSL curves for $CaSO_4$:Mn,Tb

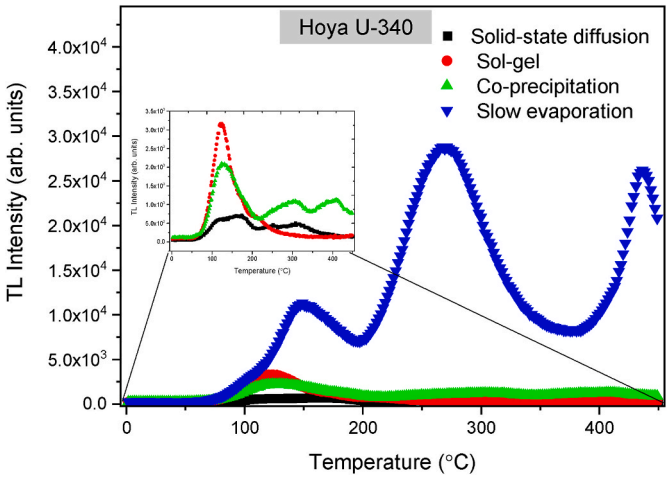

Fig. 4. TL emission curves of $CaSO_4$:Mn,Tb samples prepared by different routes, irradiated with 1 Gy of beta radiation, using a Hoya U-340 filter.

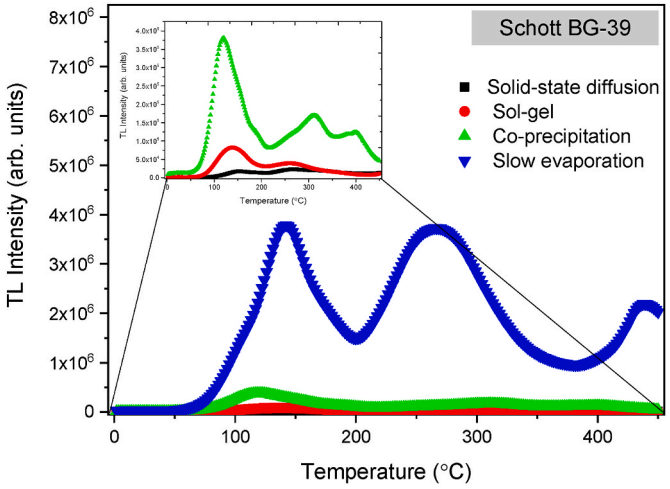

Fig. 5. TL emission curves of $CaSO_4$:Mn,Tb samples prepared by different routes, irradiated with 1 Gy of beta radiation, using a Schott BG-39 filter.

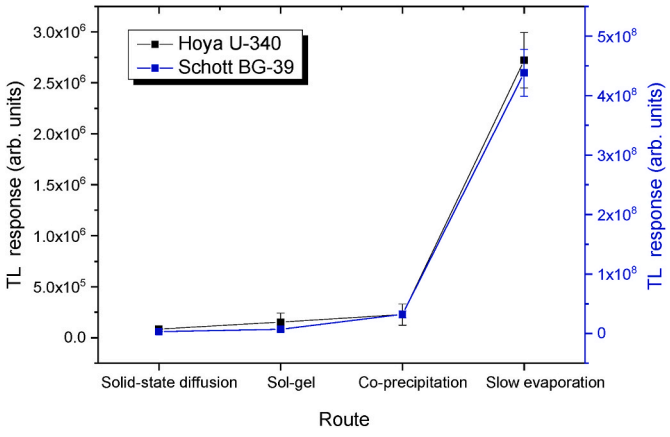

Fig. 6. TL signal obtained by integrating the area under the emission curve of $CaSO_4$:Mn,Tb samples produced by different routes, using Schott BG-39 and Hoya U-340 filters.

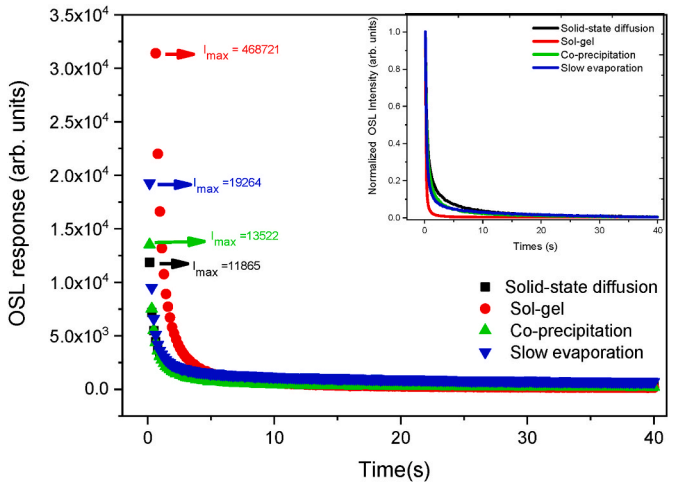

Fig. 7. OSL curves of $CaSO_4$:Mn,Tb pellets produced by different routes, irradiated with 1 Gy of $^{90}Sr/^{90}Y$. Inset: Normalized curves for comparison of decay profiles.

samples synthesized using solid-state diffusion, co-precipitation, sol-gel methods, and the slow evaporation route, with a 40 s integration time. Among the evaluated methods, the sol-gel route exhibited the highest OSL sensitivity. It yielded integrals of the OSL curves that were approximately 25 times higher than those obtained using the other synthesis methods. For all samples, the OSL signal consistently follows a trend of exponential decay as the optically active traps are emptied during stimulation. This behavior underscores the presence of traps with a high photoionization cross-section for blue LEDs (Junot et al., 2024).

Fig. 8 shows the experimental and fitted OSL decay curves. The fitting was performed using a sum of three decreasing exponential components, according to the following equation: $I_{OSL} = A_1 e^{-t/\tau_1} + A_2 e^{-t/\tau_2} + A_3 e^{-t/\tau_3}$, where A_i and τ_i (for i = 1,2,3) represent the constant coefficients associated with the fast, medium, and slow decay components, respectively; and τ_1, τ_2, and τ_3 are the corresponding decay constants, related to the probability of trapped electrons transitioning to the conduction band over time under optical stimulation, in distinct trap sets. The fitted curves reveal the presence of a fast decay component (red curve), a medium decay component (blue curve), and a slow decay component (green curve). The sum of these components (black curve) closely reproduces the experimental OSL decay behavior. It is important to emphasize that this three-component exponential fitting is a mathematical approximation aimed at ensuring consistency in the modeling process, rather than providing definitive evidence of separate underlying physical mechanisms (Altunal et al., 2018).

Table 1 presents the constant coefficients and decay constants obtained from an exponential fit of the OSL decay curves in Fig. 8. The results show a predominance of fast and medium components (A_1 and A_2), while the contribution of the slow component (A_3) was minimal, with a maximum value of only 0.110. This characteristic decay behavior, marked by an initial rapid decrease followed by a slower component, supports the presence of trapping centers with different photoionization cross sections (Daniel et al., 2016).

Table 2 further summarizes the integrals of the TL emission and OSL decay curves for $CaSO_4$:Mn,Tb compounds produced by various synthesis routes, along with uncertainties and CV values, providing insight into the luminescent performance and reproducibility of each method. The solid-state diffusion route exhibited the lowest TL and OSL responses of all filters, with moderate CV ranging from 6.04 % to 8.63 %. While this method produced samples with acceptable luminescent signal stability, the low dose sensitivity suggests a limited efficiency of the method in forming luminescent centers or suitable electron traps. The sol-gel method achieved samples with higher sensitivity values for both

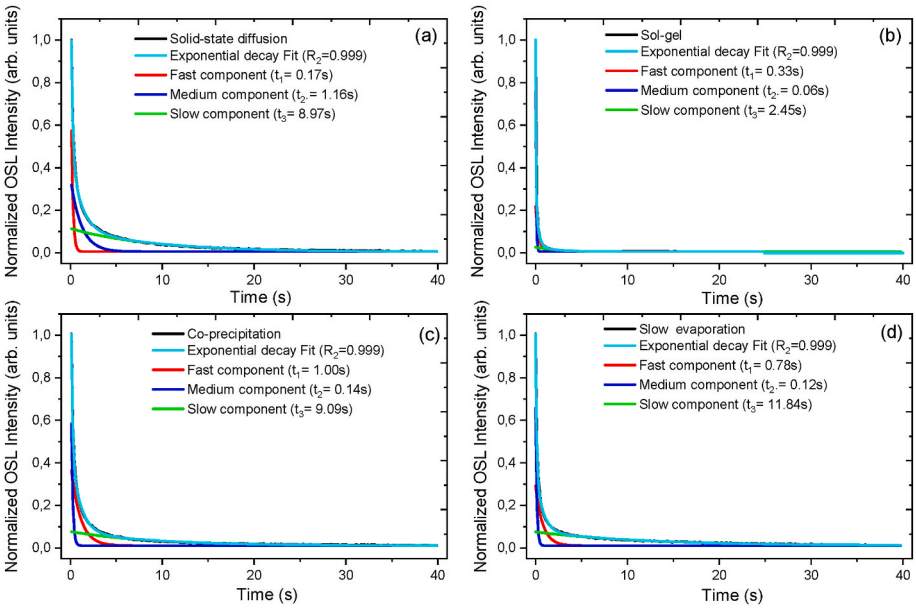

Fig. 8. Experimental and fitted OSL decay curves of $CaSO_4$:Mn,Tb samples synthesized by (a) solid-state diffusion, (b) sol-gel method, (c) co-precipitation, and (d) slow evaporation method.

Table 1
OSL parameters obtained from the exponential fit of the curves of $CaSO_4$:Mn,Tb phosphors produced by different routes.

Route	CW-OSL COMPONENT	COEFFICIENT Ai	DECAY CONSTANT τ_i (s)
Solid-state diffusion	Fast	1.446 ± 0.017 (A_1)	0.172 ± 0.003 (τ_1)
	Medium	0.362 ± 0.007 (A_2)	1.167 ± 0.029 (τ_2)
	Slow	0.110 ± 0.002 (A_3)	8.971 ± 0.144(τ_3)
Sol-gel	Fast	0.345 ± 0.008 (A_1)	0.331 ± 0.005(τ_1)
	Medium	9.172 ± 0.170 (A_2)	0.064 ± 0.001(τ_2)
	Slow	0.023 ± 0.001 (A_3)	2.456 ± 0.065(τ_3)
Co-precipitation	Fast	0.415 ± 0.008 (A_1)	1.004 ± 0.021 (τ_1)
	Medium	1.723 ± 0.025 (A_2)	0.146 ± 0.002(τ_2)
	Slow	0.067 ± 0.001 (A_3)	9.092 ± 0.206 (τ_3)
Slow evaporation	Fast	2.388 ± 0.007 (A_1)	0.168 ± 0.018 (τ_1)
	Medium	0.285 ± 0.031 (A_2)	1.215 ± 0.006 (τ_2)
	Slow	0.090 ± 0.001 (A_3)	15.18 ± 0.172 (τ_3)

TL and OSL measurements. For instance, the TL response under the BG-39 filter reached the highest TL intensity, with a low CV of 1.92 %, indicating good reproducibility in this region. However, in the UV region, the TL measurements showed a significantly high CV of 57.37 %, reflecting substantial variability in sample performance produced by the sol-gel method. Similarly, OSL measurements exhibited a CV of 18.03 %, further highlighting inconsistencies in the luminescent behavior of the samples synthesized by this route.

The co-precipitation route resulted in samples with moderate sensitivity to dose, whose TL response is characterized by high CV values, indicating inconsistencies in the material's luminescent properties. Despite this, the samples produced by this method showed a better performance in OSL measurements, achieving a lower CV of 9.54 %, which suggests improved reproducibility in this aspect compared to its TL response. The slow evaporation route stands out as the most effective and reliable synthesis method. It achieved the highest TL and OSL sensitivities across all filters, combined with relatively low CV values of 9.01 % for TL and 5.34 % for OSL indicating excellent reproducibility. These findings underscore the ability of the slow evaporation route to produce materials with superior structural homogeneity and optimized electron trap formation, resulting in enhanced sensitivity and consistent performance.

Discrepancies were observed between the TL and OSL emissions in the UV region. Samples produced by the slow evaporation method exhibited stronger TL signals, while those produced by the sol-gel route exhibited a significantly higher OSL response. This behavior can be attributed, in part, to differences in trap distributions and photoionization dynamics induced by the synthesis method. As mentioned in the TL

Table 2
Integrals of the TL emission and OSL decay curves of the produced compounds, respective uncertainties (deviation), and the percentage variation coefficients of the readings (CV).

Route	TL				OSL	
	BG-39		Hoya U-340		Hoya U-340	
	Response (arb. units)	CV (%)	Response (arb. units)	CV (%)	Response (arb. units)	CV (%)
Solid-state diffusion	(3.15 ± 0.19)x10^6	6.04	(8.50 ±0. 58) x10^4	6.84	(1.85 ± 0.16) x10^5	8.63
Sol-gel	(6.94 ± 0.13)x10^6	1.92	(1.53 ± 0.87)x10^5	57.37	(1.27 ± 0.23) x10^6	18.03
Co-precipitation	(3.23 ± 0.57)x10^7	17.84	(2.26 ± 1.03)x10^5	45.59	(1.43 ± 0.13) x10^5	9.54
Slow evaporation	(4.38 ± 0.39)x10^8	9.01	(2.72 ± 0.27)x10^6	9.97	(3.07 ± 0.16) x10^5	5.34

section, the TL signals in the UV region indicate that the synthesis of $CaSO_4$:Mn,Tb via the sol-gel route promotes the formation of shallow traps. These traps, although less thermally stable and therefore less prominent in TL measurements, can enhance the OSL response due to their higher photoionization cross-sections. McKeever et al. (1997) also showed that shallow traps can strongly affect the shape of OSL curves in the case of complex systems. Additionally, differences in crystallinity, particle size, and surface morphology, which are induced by each synthesis route, may influence the optical absorption and stimulation efficiency.

To assess the linearity of the luminescent response as a function of absorbed dose, $CaSO_4$:Mn,Tb samples were irradiated with increasing doses ranging from 0.16 to 100 Gy for both TL and OSL measurements, using a Hoya U-3540 optical filter. The integrated signals from each experimental cycle were obtained from the total luminescence counts, and the results are presented in Fig. 9 on a log–log scale as a function of dose. Both TL and OSL responses exhibit an increasing trend with dose, confirming the efficiency of these materials in detecting ionizing radiation. Moreover, the results demonstrate that the synthesis route has a direct influence on the sensitivity and linearity of the TL/OSL responses. Among the investigated routes, the slow evaporation method yielded the highest TL sensitivity and excellent linearity ($R^2 = 0.99$) for both TL and OSL. In contrast, although the sol–gel samples presented lower linearity ($R^2 = 0.913$ for TL and 0.653 for OSL), they exhibited the highest OSL sensitivity. Samples synthesized by solid-state diffusion and co-precipitation showed linear behavior and moderate luminescent intensities, lower than those obtained via slow evaporation and sol–gel, but still suitable for dosimetric applications within the analyzed dose range.

Fig. 10 displays the fading behavior of $CaSO_4$:Mn,Tb samples prepared using different synthesis routes and irradiated with 1 Gy of β-radiation, comparing TL signals measured with a Hoya U-340 filter and OSL signals recorded 15 days after irradiation. The results are presented relative to signals measured immediately after irradiation, normalized to 1.0 (black bar). All synthesis methods exhibited some degree of signal loss, reflecting charge-carrier instability, mainly associated with shallow traps. The sol–gel route showed the most pronounced fading, with 71.9 % loss in TL and 92.7 % in OSL, indicating poor charge retention. In contrast, the slow evaporation method resulted in the lowest fading, with only 11.2 % loss in TL and 41.5 % in OSL, suggesting that this route favors the formation of more stable trapping centers. It is important to note that this analysis considers the contribution of all trap levels, since the TL signal was integrated up to 450 °C. For comparison, $CaSO_4$:Mn samples exhibited higher fading rates, with 75 % loss in TL intensity and 63.6 % in OSL after 28 days, as reported by Silva et al. (2023). These results indicate that Tb^{3+} co-doping enhances charge-carrier retention, thereby improving signal stability.

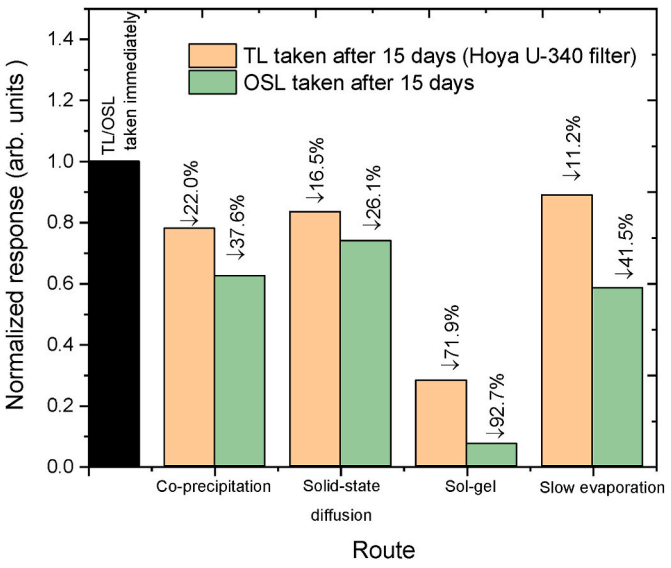

Fig. 10. Fading of $CaSO_4$:Tb,Mn after 15 days: TL with Hoya U-340 filters, and OSL. The first bar corresponds to the TL/OSL signal measured immediately after irradiation (normalized to 1); percentage losses indicated.

4. Conclusions

This study systematically evaluated the impact of four different synthesis methods (solid-state diffusion, co-precipitation, sol-gel, and slow evaporation) on the structural, morphological, and luminescent (TL and OSL) properties of $CaSO_4$:Mn,Tb phosphors. All methods resulted in samples with a $CaSO_4$ crystal phase, and the crystals produced successfully incorporated the dopants. Morphological analyses revealed significant differences among the phosphors produced by the four routes. These differences directly affected the TL and OSL responses. The phosphors obtained via the slow evaporation route exhibited the most stable and intense TL emission. In contrast, those produced by the sol-gel method yielded the highest OSL sensitivity, though with lower reproducibility compared to the samples synthesized via the slow evaporation route. The phosphors obtained via the co-precipitation and solid-state methods exhibited intermediate and less efficient luminescent properties, respectively. These findings underscore the key role of synthesis conditions in tailoring the microstructure of $CaSO_4$:Mn,Tb and enhancing its dosimetric performance. The results indicate that the slow evaporation route is a reliable and efficient method for producing $CaSO_4$:Mn,Tb phosphors for radiation dosimetry applications, offering superior TL/OSL linearity, high sensitivity, and enhanced long-term signal stability. The consistent luminescent response observed in both the visible and UV regions further broadens the applicability of these materials, underscoring the effectiveness of the slow evaporation method in optimizing their performance for a wide range of dosimetric applications. Overall, the newly synthesized $CaSO_4$:Mn,Tb phosphors exhibit promising characteristics for accurate and reproducible radiation dose evaluation.

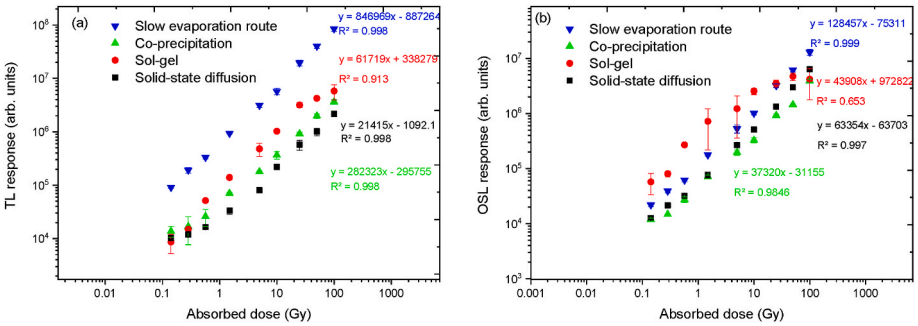

Fig. 9. TL/OSL responses of $CaSO_4$:Mn,Tb phosphors produced by different routes, as a function of absorbed dose of beta radiation.

CRediT authorship contribution statement

Anderson M.B. Silva: Writing – review & editing, Writing – original draft, Resources, Project administration, Methodology, Investigation, Formal analysis, Conceptualization. **Danilo O. Junot:** Visualization, Investigation. **Patrícia L. Antonio:** Visualization, Investigation. **Divanizia N. Souza:** Visualization, Validation, Supervision, Project administration. **Linda V.E. Caldas:** Visualization, Supervision, Resources, Project administration, Funding acquisition.

Declaration of competing interest

The authors declare the following financial interests/personal relationships which may be considered as potential competing interests: Anderson Manoel Bezerra da Silva reports financial support was provided by State of Sao Paulo Research Foundation. This work was conducted with funding from FAPESP under Project No. 2023/04859-8, granted to the author Anderson Manoel Bezerra da Silva. If there are other authors, they declare that they have no known competing financial interests or personal relationships that could have appeared to influence the work reported in this paper.

Acknowledgments

The authors gratefully acknowledge the support of the Brazilian agencies: Fundação de Amparo à Pesquisa do Estado de São Paulo (FAPESP, Projects: 2023/04859-8; 2018/05982–0 and 2022/13430-2); Conselho Nacional de Desenvolvimento Científico e Tecnológico (CNPq, Projects: 305142/2021-6, 405536/2023-2, and 406761/2022-1); and Comissão Nacional de Energia Nuclear (CNEN, Project: 1342.005453/2023–19). The authors also acknowledge the Multiuser Analysis Center of IPEN for providing access to EDS/SEM measurements.

Data availability

Data will be made available on request.

References

Altunal, V., Yegingil, Z., Tuken, T., Depci, T., Ozdemir, A., Guckan, V., Nur, N., Kurt, K., Bulur, E., 2018. Optically stimulated luminescence characteristics of BeO nanoparticles synthesized by sol-gel method. Opt. Mater. 58, 497–503. https://doi.org/10.1016/j.optmat.2016.06.019.

Aboelezz, E., Bortolin, E., Quattrini, M.C., Della, Monaca S., 2022. TL and OSL studies on irradiated nano barium strontium sulfate to photons, electrons and protons. J. Lumin. 242, 118592. https://doi.org/10.1016/j.jlumin.2021.118592.

Bahl, S., Kumar, V., Bihari, R.R., Kumar, P., 2017. Investigations of OSL properties of $CaSO_4$:Mn phosphor exposed to gamma and beta radiations. J. Lumin. 181, 36–43. https://doi.org/10.1016/j.jlumin.2016.09.004.

Bastani, S., Oliveira, L.C., Yukihara, E.G., 2019. Development and characterization of lanthanide-doped $CaSO_4$ for temperature sensing applications. Opt. Mater. 92, 273–283. https://doi.org/10.1016/j.optmat.2019.04.022.

Daniel, D.J., Raja, A., Madhusoodanan, U., Annalakshmi, O., Ramasamy, P., 2016. OSL studies of alkali fluoroperovskite single crystals for radiation dosimetry. Opt. Mater. 58, 497–503. https://doi.org/10.1016/j.optmat.2016.06.019.

Dhoble, S.J., Shahare, D.I., Moharil, S.V., 2003. Synthesis and characterization of Li_2SO_4: P,RE (RE=Dy or Eu), low Z, TLD phosphors. Phys. Stat. Sol. A. 198, 183. https://doi.org/10.1002/pssa.200306591.

Gaikwad, S.U., Patil, R.R., Kulkarni, M.S., Bhatt, B.C., Moharil, S.V., 2016. Thermoluminescence and optically stimulated luminescence in various phases of doped Na_2SO_4. Phase Trans 89, 202–210. https://doi.org/10.1080/01411594.2015.1065494.

Guckan, V., Altunal, V., Nur, N., Depci, T., Ozdemir, A., Kurt, K., Yu, Y., Yegingil, I., Yegingil, Z., 2017. Studying $CaSO_4$:Eu as an OSL phosphor. Nucl. Instrum. Methods Phys. Res. B: Beam Interact. Mater. At. 407, 145–154. https://doi.org/10.1016/j.nimb.2017.06.010.

Junot, D.O., Galeano, D.C., Silva, A.M., Souza, D.N., Caldas, L.V.E., 2024. Development of $CaSO_4$:RE,Li (RE= Tm, Eu, Tb) composites for thermally or optically stimulated luminescence dosimetry. Radiat. Meas., 107217 https://doi.org/10.1016/j.radmeas.2024.107217.

Junot, D.O., Santos, A.G., Antonio, P.L., Rezende, M.V., Souza, D.N., Caldas, L.V.E., 2019. Dosimetric and optical properties of $CaSO_4$:Tm and $CaSO_4$: tm, Ag crystals produced by a slow evaporation route. J. Lumin. 210, 58–65. https://doi.org/10.1016/j.jlumin.2019.02.005.

Junot, D.O., Souza, D.N., Caldas, L.V.E., 2020. TL/OSL signal of $CaSO_4$: Eu, Ag samples produced by variations of the slow evaporation route. Radiat. Meas. 135, 106334. https://doi.org/10.1016/j.radmeas.2020.106334.

Junot, D.O., Barros, J.P., Caldas, L.V.E., Souza, D.N., 2016. Thermoluminescent analysis of $CaSO_4$:Tb,Eu crystal powder for dosimetric purposes. Radiat. Meas. 90, 228–232. https://doi.org/10.1016/j.radmeas.2016.01.020.

Junot, D.O., Santos, M.A.C., Antonio, P.L., Caldas, L.V.E., Souza, D.N., 2014. Feasibility study of $CaSO_4$:Eu, $CaSO_4$:Eu,Ag and $CaSO_4$:Eu,Ag(NP) as thermoluminescent dosimeters. Radiat. Meas. 71, 99–103. https://doi.org/10.1016/j.radmeas.2014.05.022.

Junot, D.O., Vasconcelos, D.F., Chagas, M.A.P., Santos, M.A.C., Caldas, L.V.E., Souza, D.N., 2011. Silver addition in $CaSO_4$:Eu, TL and TSEE properties. Radiat. Meas. 46, 1500–1502. https://doi.org/10.1016/j.radmeas.2011.06.049.

Kadari, A., Mahi, K., Mostefa, R., Badaoui, M., Mameche, A., Kadri, D., 2016. Optical and structural properties of Mn doped $CaSO_4$ powders synthesized by sol-gel process. J. Alloys Compd. 688, 32–36. https://doi.org/10.1016/j.jallcom.2016.07.040.

Lakshmanan, A., Kim, S.B., Kum, B.G., Jang, H.M., Kang, B.K., 2006. Rare earth doped $CaSO_4$ luminescence phosphors for applications in novel displays–new recipes. Phys. Status Solidi. 203, 565–577. https://doi.org/10.1002/pssa.200521159.

McKeever, S.W.S., Bøtter-Jensen, L., Larsen, N.A., Duller, G.A.T., 1997. Temperature dependence of OSL decay curves: experimental and theoretical aspects. Radiat. Meas. 27, 161–170. https://doi.org/10.1016/S1350-4487(96)00106-0.

More, Y.K., Patil, R.R., Wankhede, S.P., Kulkarni, M.S., Kumar, M., Bhatt, B.C., Moharil, S.V., 2015. Optically stimulated luminescence in K_2SO_4:AEu (A= Ca, Na, Al). In: AIP Conf. Proc., 1675. https://doi.org/10.1063/1.4929180.

Nair, G.B., Swart, H.C., Dhoble, S.J., 2020. A review on the advancements in phosphorconverted light emitting diodes (pc-LEDs): phosphor synthesis, device fabrication and characterization. Prog. Mater. Sci. 109, 100622. https://doi.org/10.1016/j.pmatsci.2019.100622.

Najar, F.A., Bhat, B.H., Naik, M.M., Mir, F.A., Vakil, G.B., 2023. Effect of rare-earth Eu^{3+} and Tb^{3+} ions on the optoelectrical parameters of lithium sulfate monohydrate crystals. Opt. Quant. Electron. 55 (5), 421. https://doi.org/10.21203/rs.3.rs-1653474/v1.

Poston, J.W., 2003. Dosimetry. In: Meyers, R.A. (Ed.), Encyclopedia of Physical Science and Technology, third ed. Academic Press, pp. 603–650. https://doi.org/10.1016/B0-12-227410-5/00185-X.

Rani, R.S., Lakshmanan, A.R., Sivakumar, V., Venkatasamy, R., Annalakshmi, O., Jose, M.T., Marimuthu, K.N., 2015. Redox and charge transfer processes and luminescence in $CaSO_4$:Zn,Mn. Radiat. Meas. 76, 1350–4487. https://doi.org/10.1016/j.radmeas.2015.03.001.

Salah, N., Sahare, P.D., Lochab, S.P., Kumar, P., 2006. TL and PL studies on CaSO4:Dy nanoparticles. Radiat. Meas. 41 (1), 40–47.

Sen, D., Bahl, S., Seth, P., Singh, B., Pandey, A., Zulfequar, M., Kandasami, A., 2024. Effect of helium ion and gamma irradiation on the TL and OSL properties of Tb-doped LiF nanophosphors. J. Lumin. 271, 120587. https://doi.org/10.1016/j.jlumin.2024.120587.

Silva, A.M.B., Souza, L.F., Antonio, P.L., Junot, D.O., Caldas, L.V.E., Souza, D.N., 2022. Effects of manganese and terbium on the dosimetric properties of $CaSO_4$. Radiat. Phys. Chem. 198, 110207. https://doi.org/10.1016/j.radphyschem.2022.110207.

Silva, A.M.B., Junot, D.O., Caldas, L.V.E., Souza, D.N., 2020. Structural, optical and dosimetric characterization of $CaSO_4$:Tb, $CaSO_4$:Tb,Ag and $CaSO_4$:Tb,Ag(NP). J. Lumin. 224, 117286. https://doi.org/10.1016/j.jlumin.2020.117286.

Silva, A.M.B., Rodrigues, D.S., Antonio, P.L., Junot, D.O., Caldas, L.V.E., Souza, D.N., 2023. Investigation of dosimetric properties of $CaSO_4$:Mn phosphor prepared using slow evaporation route. Appl. Radiat. Isot. 199, 110874. https://doi.org/10.1016/j.apradiso.2023.110874.

Silva, A.M.B., Silveira, W.S., Matos, T.S., Junot, D.O., Rezende, M.V., Souza, D.N., 2021. Effect of terbium and silver co-doping on the enhancement of photoluminescence in $CaSO_4$ phosphors. Opt. Mater. 111, 110717. https://doi.org/10.1016/j.optmat.2020.110717.

Silva, A.M.B., Rodrigues, D.S., Guedes, B.D., Silveira, I.S., Antonio, P.L., Junot, D.O., Caldas, L.V.E., Souza, D.N., 2024. Exploring the luminescence properties and dosimetric characteristics of $CaSO_4$:Tb, $CaSO_4$: mn, and $CaSO_4$:Mn, Tb phosphors synthesized by slow evaporation route. Radiat. Meas. 177, 107261. https://doi.org/10.1016/j.radmeas.2024.107261.

Silva, A.M.B., Souza, D.N., Caldas, L.V.E., 2025. Thermoluminescence and optically stimulated luminescence of $CaSO_4$:Mn,Tb with different dopant concentrations. Radiat. Phys. Chem. 237, 113032. https://doi.org/10.1016/j.radphyschem.2025.113032.

Tang, Q., Zhang, C.X., Luo, D.L., Leung, P.L., Xiong, Z.Y., 2006. TL and OSL of $SrSO_4$ phosphors doped with Eu. Radiat. Protect. Dosim. 119, 238–243. https://doi.org/10.1093/rpd/nci578.